Propagation Characteristics of Magneto-Ionic Plasma Columns[1]

D. Formato and A. Gilardini

Contribution from SELENIA S.p.A., Via Tiburtina Km 12,400, Rome, Italy

The propagation characteristics of uniform, cylindrical plasma columns of circular cross section in axial, constant magnetic fields are determined. The ratios (plasma wavelength)/(free-space wavelength) and (power flowing in the plasma)/(power flowing outside) are evaluated and discussed as functions of the diameter/wavelength ratio and of the plasma permittivity, for propagation of circularly symmetrical modes. Brillouin diagrams are also derived and compared with the results predicted by the quasi-static approximation. The analysis is for a nonattenuating plasma, but formulas giving the attenuation due to electron-molecule collisions are also included.

1. Introduction

A magneto-ionic cylindrical plasma column in a static axial magnetic field may efficiently propagate an electromagnetic wave. This fact may be of importance in interpreting phenomena like plasma oscillations and atmospherics, and in designing new methods for plasma diagnostics and millimeter wave generation.

Whereas various authors have derived the characteristic equation both for a straight column of circular cross section [Akhiezer et al., 1958] and for an infinite slab [Schumann, 1958] of uniform plasma, no detailed discussion of the propagation characteristics is given, except under the so-called "quasi-static" approximation [Smullin and Chorney, 1958; Trivelpiece and Gould, 1959].

In such an approximation the propagation wavelength must be much less than the free-space wavelength, a condition usually fulfilled only when plasma transverse dimensions are much smaller than the free-space wavelength.

Our analysis, instead, is concerned with the solution of the exact characteristic equation, written for the propagation of circularly symmetrical modes in a uniform, nonattenuating plasma of circular cross section; the permittivity tensor is chosen as constant parameter for each solution. We have found it convenient to plot our results as the ratios (plasma wavelength)/(free space wavelength) and (power flowing in the plasma)/(power flowing outside) versus the diameter/wavelength ratio.

Using these results we have also derived the plots of angular frequency versus wave number for each mode (Brillouin diagrams), assuming constant values for the plasma and cyclotron frequencies. These diagrams are similar to those obtained using the quasi-static approximation, except for a few features, which will be described.

A final section is devoted to the attenuation formulas, when the electron-molecule collisions are taken into consideration.

2. Plasma Dielectric Constant

The dielectric constant of a uniform plasma in a constant magnetic field $\vec{B}$ is a tensor $\|\epsilon\|$, defined by the relationship:

$$D_i = \epsilon_{il} E_l \tag{1}$$

where $\vec{D}$ is the electric displacement and $\vec{E}$ is the electric field.

If the field $\vec{B}$ is directed along the positive z axis $(i, l=3)$, the ϵ_{il} components due to the electron motion alone are given, for zero agitation and drift velocities, by the expressions [Allis, 1956]:

$$\left.\begin{aligned}
\epsilon_{11} &= \epsilon_{22} = \epsilon_0(\epsilon_1 - j\epsilon_1'') = \epsilon_0\left[1 + \frac{\omega_p^2}{2j\omega[\nu_c + j(\omega - \omega_b)]} + \frac{\omega_p^2}{2j\omega[\nu_c + j(\omega + \omega_b)]}\right] \\
\epsilon_{33} &= \epsilon_0(\epsilon_3 - j\epsilon_3'') = \epsilon_0\left[1 + \frac{\omega_p^2}{j\omega(\nu_c + j\omega)}\right] \\
\epsilon_{12} &= -\epsilon_{21} = j\epsilon_0(\epsilon_2 - j\epsilon_2'') = \epsilon_0\frac{\omega_p^2}{2\omega}\left[\frac{1}{\nu_c + j(\omega - \omega_b)} - \frac{1}{\nu_c + j(\omega + \omega_b)}\right] \\
\epsilon_{13} &= \epsilon_{23} = \epsilon_{31} = \epsilon_{32} = 0.
\end{aligned}\right\} \quad (2)$$

Here ν_c is the electron collision frequency (assumed to be velocity independent), ω is the angular frequency of the applied field (well above the ion gyrofrequencies, so that the ion contributions may be neglected), ω_p is the angular plasma frequency ($=\sqrt{ne^2/m\epsilon_0}$, n being the electron density, m and e the electron mass and charge, and ϵ_0 the free space permittivity) and ω_b is the angular cyclotron frequency ($=eB/m$).

When $\nu_c^2 \ll \omega^2$ and $\nu_c^2 \ll (\omega - \omega_b)^2$, the above formulas become:

$$\left.\begin{aligned}
\epsilon_1 - j\epsilon_1'' &= 1 + \frac{\omega_p^2}{\omega_b^2 - \omega^2} - j\nu_c\frac{\omega_p^2(\omega_b^2 + \omega^2)}{\omega(\omega_b^2 - \omega^2)^2} \\
\epsilon_2 - j\epsilon_2'' &= \frac{\omega_b}{\omega}\frac{\omega_p^2}{\omega_b^2 - \omega^2} - j\nu_c\frac{2\omega_p^2\omega_b}{(\omega_b^2 - \omega^2)^2} \\
\epsilon_3 - j\epsilon_3'' &= 1 - \frac{\omega_p^2}{\omega^2} - j\nu_c\frac{\omega_p^2}{\omega^3}.
\end{aligned}\right\} \quad (3)$$

Since the collision frequency ν_c is proportional to the gas pressure, the above inequalities are fulfilled, whenever the pressure is sufficiently low; we assume throughout the paper that this is always the case.
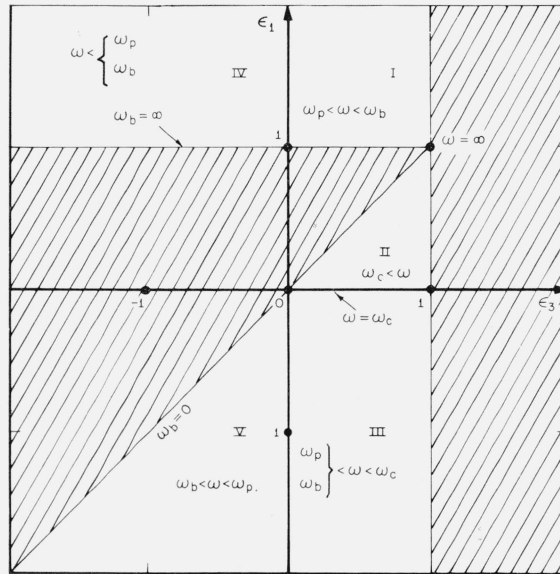

FIGURE 1. *Regions of permitted and forbidden ϵ_1 and ϵ_3 values.*

The propagation characteristics will be first investigated assuming $\nu_c = 0$ (and then $\epsilon_1'' = \epsilon_2'' = \epsilon_3'' = 0$), a condition which provides propagation without losses. Later we shall compute the losses, removing this assumption, but still considering the ϵ'' terms small compared to the ϵ ones.

From (3) one can derive the following relationship between ϵ_1, ϵ_2, ϵ_3:

$$\epsilon_2^2 = (\epsilon_1 - 1)(\epsilon_1 - \epsilon_3). \tag{4}$$

It is convenient to assume ϵ_1 and ϵ_3 as the independent variables of our problem. These dielectric constant components are functions of ω, ω_p and ω_b; the range of values that ϵ_1 and ϵ_3 may have is shown in figure 1. In this figure we have divided the plane of possible values in five regions: a separate discussion of the propagation characteristics will be presented for each region. In the figure a new convenient frequency ω_c, defined as $\sqrt{\omega_p^2 + \omega_b^2}$, has also been introduced.

3. Propagation in a Cylindrical Column

We assume a cylindrical plasma of circular cross section in an infinite free space. The plasma is uniform and in steady state conditions; its axis is parallel to the static magnetic field direction (z=axis). Our analysis is here limited to the propagation of circularly symmetrical modes, namely to the propagation of fields without azimuthal dependence.

In a cylindrical orthogonal system of coordinates (ρ,φ,z) these fields are [Epstein, 1956] inside the plasma:

$$\left.\begin{aligned}
&E_z = A_1 J_0(x_1\rho/R) + A_2 J_0(x_2\rho/R) \\
&E_\rho = -j\frac{2\pi R}{\lambda_0}\left\{\frac{\epsilon_2}{\epsilon_1}\left[A_1\frac{g_1}{x_1}J_1(x_1\rho/R) + A_2\frac{g_2}{x_2}J_1(x_2\rho/R)\right]\right. \\
&\qquad\qquad\qquad \left.-\frac{\epsilon_3}{\epsilon_1}\alpha\left[A_1\frac{1}{x_1}J_1(x_1\rho/R) + A_2\frac{1}{x_2}J_1(x_2\rho/R)\right]\right\} \\
&E_\varphi = \frac{2\pi R}{\lambda_0}\left[A_1\frac{g_1}{x_1}J_1(x_1\rho/R) + A_2\frac{g_2}{x_2}J_1(x_2\rho/R)\right] \\
&H_z = j\frac{1}{Z_0}[A_1 g_1 J_0(x_1\rho/R) + A_2 g_2 J_0(x_2\rho/R)] \\
&H_\rho = -\frac{2\pi R}{\lambda_0}\frac{\alpha}{Z_0}\left[A_1\frac{g_1}{x_1}J_1(x_1\rho/R) + A_2\frac{g_2}{x_2}J_1(x_2\rho/R)\right] \\
&H_\varphi = j\frac{2\pi R}{\lambda_0}\frac{\epsilon_3}{Z_0}\left[A_1\frac{1}{x_1}J_1(x_1\rho/R) + A_2\frac{1}{x_2}J_1(x_2\rho/R)\right]
\end{aligned}\right\} \tag{5}$$

outside the plasma:

$$\left.\begin{aligned}
&E_z = BK_0(x_0\rho/R) \\
&E_\rho = -j\frac{2\pi R}{\lambda_0}\alpha\cdot B\frac{1}{x_0}K_1(x_0\rho/R) \\
&E_\varphi = -\frac{2\pi R}{\lambda_0}C\frac{1}{x_0}K_1(x_0\rho/R) \\
&H_z = j\frac{1}{Z_0}CK_0(x_0\rho/R) \\
&H_\rho = \frac{2\pi R}{\lambda_0}\frac{\alpha}{Z_0}C\frac{1}{x_0}K_1(x_0\rho/R) \\
&H_\varphi = -j\frac{2\pi R}{x_0}\frac{1}{Z_0}B\frac{1}{x_0}K_1(x_0\rho/R)
\end{aligned}\right\} \tag{6}$$

where

$$R = \frac{d}{2} = \text{radius of the plasma cylinder}$$

$$\alpha = \frac{\lambda_0}{\lambda_g} = \text{free space } \lambda_0 \text{ to guided } \lambda_g \text{ wavelength ratio}$$

$$Z_0 = \text{free space characteristic impedance}$$

$J_0, J_1, K_0, K_1 = $ Bessel functions, according to McLachlan symbolism [McLachlan, 1955].

$$\left.\begin{aligned}
x_{1,2} &= \frac{2\pi R}{\lambda_0}\, \delta_{1,2}(\alpha^2-1)^{\frac{1}{2}} = \delta_{1,2}x_0 \\[2mm]
x_0 &= \frac{2\pi R}{\lambda_0}\,(\alpha^2-1)^{\frac{1}{2}} \\[2mm]
\delta_{1,2}^2 &= \frac{\epsilon_3(\epsilon_1-\alpha^2)}{\epsilon_1(\alpha^2-1)} + \frac{\epsilon_1-\epsilon_3}{2\epsilon_1}\left[-1 \pm \sqrt{1+4\,\frac{\epsilon_3(\epsilon_1-1)}{\epsilon_1-\epsilon_3}\,\frac{\alpha^2}{(\alpha^2-1)^2}}\,\right] \\[2mm]
g_{1,2} &= \frac{\epsilon_1\delta_{1,2}^2(\alpha^2-1)-\epsilon_3(\epsilon_1-\alpha^2)}{\alpha\epsilon_2}.
\end{aligned}\right\} \tag{7}$$

It is desired that the fields outside the plasma decay radially to zero at infinity. Since K_0 is analogous to a negative exponential only when the argument is real positive, then x_0 must be real, and consequently $\alpha^2 > 1$.

The condition that the tangential fields be continuous at the plasma boundary gives the following transcendental equation, which determines the unknown quantity α^2:

$$F(x_0,\delta_2,\epsilon_3) = \tau F(x_0,\delta_1,\epsilon_3), \tag{8}$$

where

$$F(x_0,\delta,\epsilon_3) = \frac{\dfrac{1}{\delta}\dfrac{J_1(\delta x_0)}{J_0(\delta x_0)} + \dfrac{K_1(x_0)}{K_0(x_0)}}{\dfrac{\epsilon_3}{\delta}\dfrac{J_1(\delta x_0)}{J_0(\delta x_0)} + \dfrac{K_1(x_0)}{K_0(x_0)}}. \tag{9}$$

$$\tau = \frac{g_1}{g_2} = \frac{1-\sqrt{1+4\epsilon_3(\epsilon_1-1)\alpha^2/(\epsilon_1-\epsilon_3)(\alpha^2-1)^2}}{1+\sqrt{1+4\epsilon_3(\epsilon_1-1)\alpha^2/(\epsilon_1-\epsilon_3)(\alpha^2-1)^2}}. \tag{10}$$

Equation (8) is the characteristic equation of our propagation problem. Its solutions will be discussed in the next section.

4. Wavelengths in Plasma Guided Propagation

For the solution of (8) and a survey of the results it is important to know the behavior of $F(x_0,\delta,\epsilon_3)$ as a function of x_0, for different δ^2 values. This is plotted in figure 2 and in figure 3 for positive and negative ϵ_3 values respectively. Important points on the x_0 axis are $X_n^{(m)}$, $\mu^{(m)}(\delta)$, and $\nu^{(m)}(\delta,\epsilon_3)$, which are the mth nonzero solutions of the equations:

$$\left.\begin{aligned}
J_n(X_n^{(m)}) &= 0 \\[2mm]
\frac{1}{\delta}\frac{J_1(\mu^{(m)}\delta)}{J_0(\mu^{(m)}\delta)} &= -\frac{K_1(\mu^{(m)})}{K_0(\mu^{(m)})} \\[2mm]
\frac{\epsilon_3}{\delta}\frac{J_1(\nu^{(m)}\delta)}{J_0(\nu^{(m)}\delta)} &= -\frac{K_1(\nu^{(m)})}{K_0(\nu^{(m)})}
\end{aligned}\right\} \tag{11}$$

If $\delta^2 \to +\infty$, then $\mu^{(m)}$ and $\nu^{(m)} \to X_0^{(m)}/\delta \to 0$. If $\delta^2 \to 0$, $\mu^{(m)}$ and $\nu^{(m)}(\epsilon_3 > 0) \to X_1^{(m)}/\delta \to \infty$, $\nu^{(m)}(\epsilon_3 < 0) \to X_1^{(m-1)}/\delta \to \infty$ when $m \neq 1$, whereas $\nu^{(1)}(\epsilon_3 < 0)$ remains finite.

It is convenient to represent the solutions of (8) as relative wavelengths $\lambda_g/\lambda_0 = 1/\alpha$ versus d/λ_0 for different sets of ϵ_1 and ϵ_3 values. For this purpose we have proceeded as follows:

1. From a set of real ϵ_1, ϵ_3 and α^2 values the corresponding δ_1^2, δ_2^2 and τ values are computed.

2. The x_0 solutions of (8) are determined. More than one x_0 value may be found; in this case for each solution there is a different field configuration, that is called propagation mode. Since $F(x_0, +\delta, \epsilon_3) = F(x_0, -\delta, \epsilon_3)$, no sign ambiguity results in taking the square root of δ^2.

3. The corresponding d/λ_0 are obtained from the equation:

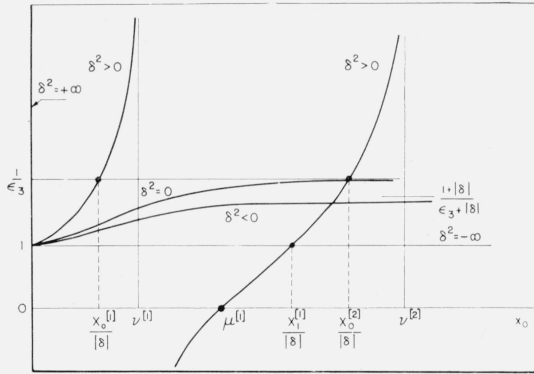$$\frac{d}{\lambda_0} = \frac{x_0}{\pi \cdot \sqrt{\alpha^2 - 1}}. \tag{12}$$

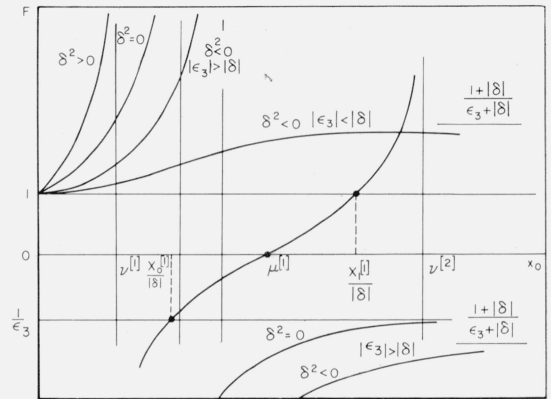FIGURE 2. *Behavior of* F *versus* x_0 *for* $\epsilon_3 > 0$ *and different* δ^2 *values.*

FIGURE 3. *Behavior of* F *versus* x_0 *for* $\epsilon_3 < 0$ *and different* δ^2 *values.*

The computations are repeated for the same ϵ_1 and ϵ_3, but for different α^2 values between unity and infinity.

The analysis of (8) for arbitrary ϵ_1 and ϵ_3 values would be unnecessarily general. We have then restricted our investigation only to the sets of values, which may be found in the five significant regions shown in figure 1. The following results have been obtained.

1. In region I (see appendix A and fig. 4) no propagation of the mth mode is possible for d/λ_0 values smaller than:

$$\left(\frac{d}{\lambda_0}\right)_c^{(m)} = \frac{X_0^{(m)}}{\pi} \left[\frac{|\epsilon_1|}{\epsilon_3|\epsilon_1 - 1| + \sqrt{\epsilon_3(\epsilon_1 - 1)(\epsilon_1 - \epsilon_3)}}\right]^{\frac{1}{2}}. \tag{13}$$

At this cutoff condition $\lambda_g = \lambda_0$; for larger d/λ_0 values propagation takes place with a λ_g continuously decreasing towards the infinite plasma value:

$$\lambda_g = \frac{\lambda_0}{\alpha_0} = \frac{\lambda_0}{[\epsilon_1 + \sqrt{(\epsilon_1 - 1)(\epsilon_1 - \epsilon_3)}]^{\frac{1}{2}}} = \frac{\lambda_0}{\sqrt{\epsilon_1 + \epsilon_2}}. \tag{14}$$

This limit represents the well-known propagation of a TEM plane uniform wave, with a right-hand circular polarization. In fact, at this limit, the E_ρ and E_φ components become equal and 90° out of phase. These curves have the same shape, as those for propagation in the dielectric waveguides; moreover, by setting $\epsilon_1 = \epsilon_3 = \epsilon$ into (13) and (14) we obtain exactly the cutoff condition and the free space propagation wavelength for dielectric waveguides, TE_{om} or TM_{om} modes.
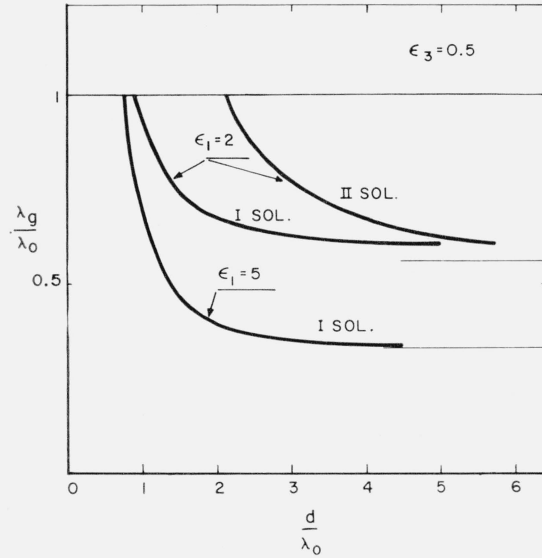
547

FIGURE 4. *Wavelength ratios* λ_g/λ_0 *versus* d/λ_0 *in region I.*
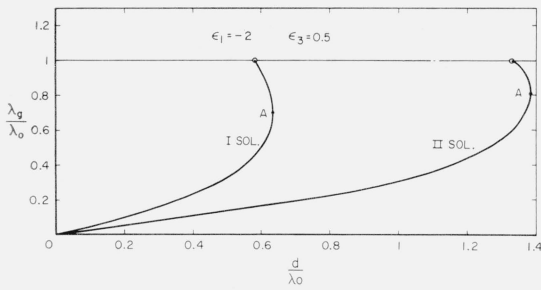
FIGURE 5. *Wavelength ratios* λ_g/λ_0 *versus* d/λ_0 *in region III.*
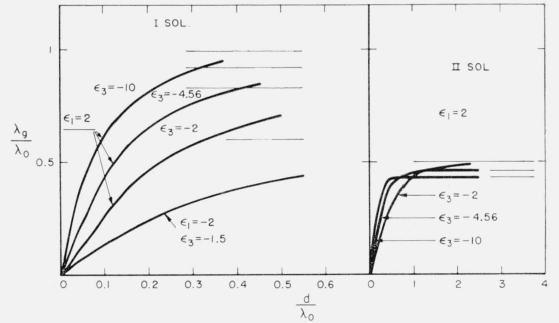
FIGURE 6. *Wavelength ratios* λ_g/λ_0 *versus* d/λ_0 *in regions IV and V.*

2. In region II no propagation is ever possible (see appendix A).

3. In region III (see appendix A and fig. 5) an infinite number of propagation modes exist. All the λ_g/λ_0 versus d/λ_0 curves start from the origin, the initial slopes being $\pi/\nu^{(m)}(\delta_\infty)$, where $\delta_\infty^2 = -\epsilon_3/\epsilon_1$. Unity wavelength ratios are attained at the same (d/λ_0), defined by (13). However, when the λ_g curves have the hook shape shown in figure 5, propagation takes place also at larger d/λ_0 ratios. In this case we have two wavelength ratios for each d/λ_0 condition; in general the group velocities of these two possible waves are opposite. The group velocity is zero at the maximum d/λ_0 (points A).

4. In region IV (see appendixes B and C and fig. 6), as in region III, an infinite number of propagation modes exist and all the λ_g/λ_0 versus d/λ_0 curves start from the origin, the initial slopes being $\pi/\nu^{(m)}(\delta_\infty)$. Here, however, propagation is possible over the entire d/λ_0 range; the curves have positive slopes and approach, as $d/\lambda_0 \to \infty$, an horizontal asymptote which is the same for all modes, except for the mode of the lowest x_0 solution.

5. In region V (see again appendixes B and C and fig. 6) we have at most one λ_g/λ_0 versus d/λ_0 curve for each pair of ϵ_1, ϵ_3 values. The curve has the same behavior as the curves found in region IV. The initial slope is $\pi/\nu^{(1)}(\delta_\infty)$. The curve may exist only if $\epsilon_1\epsilon_3 > 1$, which in the frequency domain corresponds to the $\omega_b < \omega < \omega_c/\sqrt{2} < \omega_p$ range.

The above discussed results coincide, in the $\lambda_g/\lambda_0 \ll 1$ region, with those given by the quasistatic approximation.

548

5. Brillouin Diagrams

Keeping ϵ_1 and ϵ_3 as constant parameters in the Maxwell equations, it has been possible to solve the dispersion equation using a lengthy but straightforward procedure. Brillouin diagrams $\left(\beta = \dfrac{2\pi}{\lambda_g} \text{ versus } k = 2\pi/\lambda_0 = \omega/c, \, c \text{ being the light velocity} \right)$ are, instead, more difficult to derive, because ϵ_1 and ϵ_3 are functions of frequency.

In order to obtain these diagrams from the previous section curves we must solve the following system:

$$\left. \begin{aligned} \lambda_g/\lambda_0 &= f(d/\lambda_0, \epsilon_1, \epsilon_3) \\[4pt] \epsilon_1 &= \left(1 + \frac{\omega_p^2}{\omega_b^2 - \omega^2} \right) \\[4pt] \epsilon_3 &= \left(1 - \frac{\omega_p^2}{\omega^2} \right). \end{aligned} \right\} \tag{15}$$

For this let us keep constant the ratio $a = \dfrac{\omega_b^2}{\omega_p^2}$ and choose all the pairs of ϵ_1 and ϵ_3 values, which satisfy the relationship:

$$\epsilon_1 = \frac{a(1 - \epsilon_3) - \epsilon_3}{a(1 - \epsilon_3) - 1}. \tag{16}$$

Then the first equation of the system (15) provides, in the Brillouin kd versus βd plane, a set of curves, ϵ_3, and a being constant for each curve. These curves will intercept the horizontal lines:

$$kd = k_p d / \sqrt{1 - \epsilon_3} \tag{17}$$

which represent the third equation of the above system (15), $k_p d$ being the plasma density parameter $\omega_p d/c$. For given values of the frequency independent parameters a and $k_p d$, these intercepts at different ϵ_3 values describe the Brillouin curves:

$$\beta d = F(kd, a, k_p d). \tag{18}$$

Typical Brillouin diagrams are plotted in figures 7 and 8 for $k_p d = 3.5$ and for two a values, the first chosen in the $a > 1$ region ($a = 2.25$), the second in the $a < 1$ region ($a = 0.5$).

It is interesting to compare these curves with the corresponding curves obtained by Gould and Trivelpiece [1959] and by Smullin and Chorney [1958] using the so-called quasi-static approximation. These authors have studied the more general case of a circular waveguide partially filled with plasma; from their results the curves to be used in our case are easily derived by setting the waveguide diameter equal to infinity.
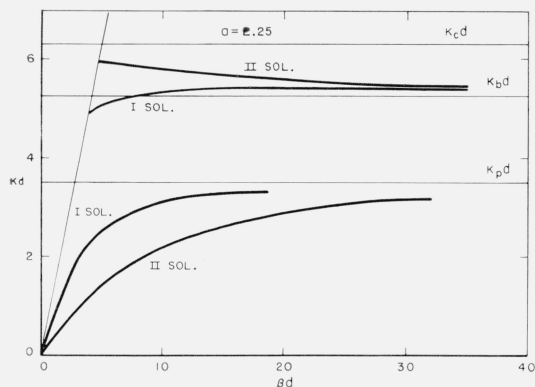
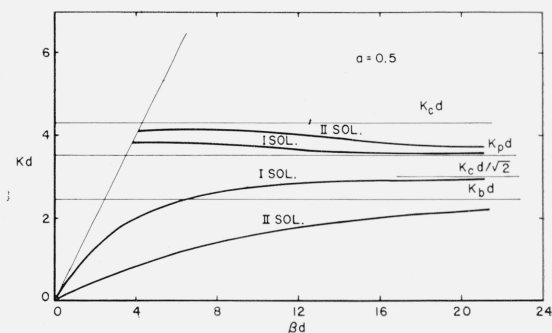FIGURE 7. *Brillouin diagrams for* a=2.25 *and* $k_p d = 3.5$.

FIGURE 8. *Brillouin diagrams for* a=0.5 *and* $k_p d = 3.5$.

No significant difference is found in the behavior of the Brillouin diagrams in the $\omega < \omega_p$ region ($kd < k_p d$). In this region all the kd versus βd curves start from the origin and approach asymptotically the value $k_p d$ or $k_b d$, whichever is smaller, except the first solution mode which, when $\omega_p > \omega_b$, approaches the asymptotic value $k_c d / \sqrt{2} = (k_p^2 d^2 + k_b^2 d^2)^{\frac{1}{2}} / \sqrt{2}$.

A behavior slightly more complicated than predicted from the quasi-static approximation is found in the $\omega > \omega_p$ region. Here the curves start from different points of the $kd = \beta d$ line between $k_p d$ and $k_c d$ and approach the asymptotic value $k_p d$ or $k_b d$, whichever is larger. The slopes of these curves may be positive, negative, or partially positive and partially negative, so that the waves can be forward or backward. It is worth noting that in the quasi-static approximation all these waves are always backward.

The following details can be added to the discussed features in the $\omega > \omega_p$ region.

(a) The starting points on the $kd = \beta d$ line are given from the simple relation:

$$kd = k_p d \frac{\sqrt{a + (1+p)^2}}{1+p} \tag{19}$$

where

$$p = [k_p d / 2 X_0^{(m)}]^2.$$

(b) When $\omega_b > \omega_p$ the wave of a given mode is always forward if:

$$k_b^2 d^2 - k_p^2 d^2 > 2 (X_1^{(m)})^2. \tag{20}$$

If this condition is not satisfied, the wave may be backward, or start at low βd values as forward and change to backward at large βd values.

For a plasma, which, instead of being stationary, has a uniform drift motion u_0 along the z axis, the Brillouin diagrams are obtained from the above ones by substituting the Doppler shifted frequency $\omega - \beta u_0$ to the signal frequency ω. Our results are thus translated into the phase characteristics of space charge and transverse field waves of an electron beam. In this way they are useful for studies of traveling-wave and parametric amplification tubes.

6. Power Flow

The power flowing inside the plasma and the power flowing outside are obtained by integration of the Poynting vector over the respective areas.

The z component of this vector inside the plasma is

$$S_z^p = \frac{\alpha D^2}{Z_0} \left(\frac{2\pi R}{\lambda_0} \right)^2 \left[\frac{N_1 G_1^2}{g_1^2 x_1^2} \frac{J_1^2(x_1 \rho/R)}{J_0^2(x_1)} + \frac{N_2 G_2^2}{g_2^2 x_2^2} \frac{J_1^2(x_2 \rho/R)}{J_0^2(x_2)} - \frac{N_3 G_1 G_2}{g_1 g_2 x_1 x_2} \frac{J_1(x_1 \rho/R)}{J_0(x_1)} \frac{J_1(x_2 \rho/R)}{J_0(x_2)} \right] \tag{21}$$

where, for symmetry and simplicity, we have introduced the new symbols:

$$\left.\begin{aligned}
D &= \frac{g_1}{G_1} J_0(x_1) A_1 \\
G_1 &= \left[\frac{1}{x_1} \frac{J_1(x_1)}{J_0(x_1)} + \frac{1}{x_0} \frac{K_1(x_0)}{K_0(x_0)} \right]^{-1} \\
G_2 &= \left[\frac{1}{x_2} \frac{J_1(x_2)}{J_0(x_2)} + \frac{1}{x_0} \frac{K_1(x_0)}{K_0(x_0)} \right]^{-1} \\
N_{1,2} &= g_{1,2}^2 + \frac{\epsilon_3^2}{\epsilon_1} - \frac{\epsilon_3 \epsilon_2}{\epsilon_1} \frac{g_{1,2}}{\alpha} = g_{1,2}^2 - \frac{\epsilon_3 (\alpha^2 - 1) \delta_{1,2}^2 - \epsilon_3^2}{\alpha^2} \\
N_3 &= 2 g_1 g_2 + 2 \frac{\epsilon_3^2}{\epsilon_1} - \frac{\epsilon_3 \epsilon_2}{\epsilon_1} \frac{g_1 + g_2}{\alpha} = - \frac{\epsilon_3 (\epsilon_1 - \epsilon_3)}{\epsilon_1} \frac{\alpha^2 + 1}{\alpha^2}.
\end{aligned}\right\} \tag{22}$$

The z component of the Poynting vector outside the plasma is

$$S_z^a = \frac{\alpha D^2}{Z_0} \left(\frac{2\pi R}{\lambda_0} \right)^2 \left[\left(\frac{G_1}{g_1} - \frac{G_2}{g_2} \right)^2 + (G_1 - G_2)^2 \right] \cdot \frac{1}{x_0^2} \frac{K_1^2(x_0 \rho/R)}{K_0^2(x_0)}. \tag{23}$$

When integrations are performed, the ratio between the inside and outside powers can be written as:

$$\frac{P_p}{P_a} = \frac{\int_0^R S_z^p \rho \, d\rho}{\int_R^\infty S_z^a \rho \, d\rho} = \left(\frac{P_p}{P_a}\right)_1 + \left(\frac{P_p}{P_a}\right)_2 + \left(\frac{P_p}{P_a}\right)_3 \tag{24}$$

where

$$\left.\begin{aligned}
\left(\frac{P_p}{P_a}\right)_1 &= \frac{N_1 G_1^2}{\delta_1^2 g_1^2 M}\left(1 - \frac{2}{x_1}\frac{J_1(x_1)}{J_0(x_1)} + \frac{J_1^2(x_1)}{J_0^2(x_1)}\right) \\
\left(\frac{P_p}{P_a}\right)_2 &= \frac{N_2 G_2^2}{\delta_2^2 g_2^2 M}\left(1 - \frac{2}{x_2}\frac{J_1(x_2)}{J_0(x_2)} + \frac{J_1^2(x_2)}{J_0^2(x_2)}\right) \\
\left(\frac{P_p}{P_a}\right)_3 &= \frac{2N_3(G_1 - G_2)}{(\delta_1^2 - \delta_2^2)g_1 g_2 M} \\
M &= \left[\left(\frac{G_1}{g_1} - \frac{G_2}{g_2}\right)^2 + (G_1 - G_2)^2\right]\left(1 + \frac{2}{x_0}\frac{K_1(x_0)}{K_0(x_0)} - \frac{K_1^2(x_0)}{K_0^2(x_0)}\right).
\end{aligned}\right\} \tag{25}$$

The three terms of (24) are respectively proportional to the power transported by the field components of amplitude A_1, by the field components of amplitude A_2 and by their mutual interaction (with reference to the expressions (5)).

The P_p/P_a ratio is always real, also in the region where δ_1^2 and δ_2^2 are complex; in fact, in this region x_1 and x_2, g_1 and g_2, N_1 and N_2, G_1 and G_2 are all complex conjugates, so that the resulting $(P_p/P_a)_1$ and $(P_p/P_a)_2$ are complex conjugates too, and their sum is real, as it is the third term $(P_p/P_a)_3$.
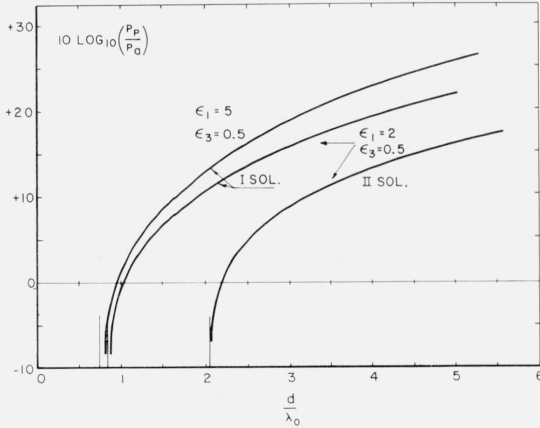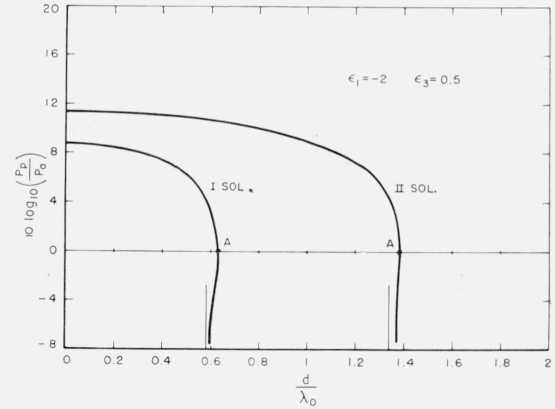

FIGURE 9. *Power flow ratios* P_p/P_a *versus* d/λ_0 *in region I.*

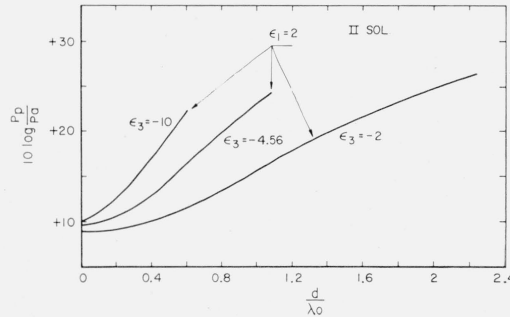FIGURE 10. *Power flow ratios* P_p/P_a *versus* d/λ_0 *in region III.*

FIGURE 11. *Power flow ratios* P_p/P_a *versus* d/λ_0 *in region IV.*

551

The ratios P_p/P_a versus d/λ_0 have been computed and plotted in figures 9, 10, and 11 for the same ϵ_1 and ϵ_3 values used in the numerical solutions of the characteristic equation, with the exception of the first solution in the $\epsilon_3 < 0$ region.

The ratios for this first solution have been evaluated in the limiting cases of zero and infinite d/λ_0 values and have resulted much smaller than unity. The practical interest of this mode seems then very scarce; for this reason the complete curves have not been evaluated.

A few more remarks seem worth mentioning:

1. The Poynting vector has also a nonzero ϕ component, so that the power is actually flowing helically around the z direction.

2. In region III the power flow inside the plasma may be backward. In this case, if $P_p > P_a$ we have an "average" backward wave, if $P_p < P_a$ an "average" forward wave. The points labeled A in figure 5, where the group velocity is zero, correspond to the points A in figure 10 where $P_p = P_a$, so that, although power is actually flowing separately inside and outside the plasma, the total flow is zero.

3. Also in region V the power flow in the plasma may be backward, although the total power is flowing forward, being $P_p P_a$.

7. Attenuation Coefficient

The attenuation coefficient a for the wave propagation is related to the power dissipated by losses per unit length P_d by the well-known formula:

$$a = \frac{1}{2} \frac{P_d}{P_p + P_a}. \tag{26}$$

We neglect the losses in the dielectric surrounding the plasma (usually air) and assume that the fields are those we have computed in the previous paragraphs, neglecting losses. In this case the losses are only due to the imaginary terms of the plasma dielectric constant and P_d is given by:

$$P_d = \text{Real}\left[j\omega \int_0^R \vec{E} \cdot \vec{D}^* 2\pi\rho d\rho \right]. \tag{27}$$

By means of (1) and (2), and recalling that E_ρ and E_φ are 90° out of phase, this becomes:

$$P_d = \omega\epsilon_0 \int_0^R [\epsilon_1''(E_\rho E_\rho^* + E_\varphi E_\varphi^*) - j\epsilon_2''(E_\rho E_\varphi^* - E_\varphi E_\rho^*) + \epsilon_3'' E_z E_z^*] 2\pi\rho d\rho. \tag{28}$$

Substituting the field expressions and performing the integrations, we finally obtain:

$$a = \frac{\pi}{\lambda_0} \left\{ \frac{W_1}{N_1}\left(\frac{P_p}{P_a}\right)_1 + \frac{W_2}{N_2}\left(\frac{P_p}{P_a}\right)_2 + \frac{W_3}{N_3}\left(\frac{P_p}{P_a}\right)_3 + \epsilon_3'' \frac{Y}{M} \frac{\alpha^2-1}{\alpha} \right\} \left(1 + \frac{P_p}{P_a}\right)^{-1} \tag{29}$$

where:

$$
\begin{aligned}
W_1 &= \epsilon_1''\left[\left(\frac{\epsilon_2^2}{\epsilon_1^2}+1\right)\frac{g_2^2}{\alpha}+\frac{\epsilon_3^2}{\epsilon_1^2}\alpha-2\frac{\epsilon_2\epsilon_3}{\epsilon_1^2}g_1\right]-2\epsilon_2''\left[\frac{\epsilon_2}{\epsilon_1}\frac{g_2^2}{\alpha}-\frac{\epsilon_3}{\epsilon_1}g_1\right] \\[6pt]
W_2 &= \epsilon_1''\left[\left(\frac{\epsilon_2^2}{\epsilon_1^2}+1\right)\frac{g_2^2}{\alpha}+\frac{\epsilon_3^2}{\epsilon_1^2}\alpha-2\frac{\epsilon_2\epsilon_3}{\epsilon_1^2}g_2\right]-2\epsilon_2''\left[\frac{\epsilon_2}{\epsilon_1}\frac{g_1^2}{\alpha}-\frac{\epsilon_3}{\epsilon_1}g_2\right] \\[6pt]
W_3 &= 2\epsilon_1''\left[\left(\frac{\epsilon_2^2}{\epsilon_1^2}+1\right)\frac{g_1 g_2}{\alpha}+\frac{\epsilon_3^2}{\epsilon_1^2}\alpha-\frac{\epsilon_2\epsilon_3}{\epsilon_1^2}(g_1+g_2)\right]-4\epsilon_2''\left[\frac{\epsilon_2}{\epsilon_1}\frac{g_1 g_2}{\alpha}-\frac{\epsilon_3}{2\epsilon_1}(g_1+g_2)\right] \\[6pt]
Y &= \frac{G_1^2}{g_1^2}\left[1+\frac{J_1^2(x_1)}{J_0^2(x_1)}\right]+\frac{G_2^2}{g_2^2}\left[1+\frac{J_1^2(x_2)}{J_0^2(x_2)}\right]-\frac{4G_1 G_2}{g_1 g_2}\frac{x_1\frac{J_1(x_1)}{J_0(x_1)}-x_2\frac{J_1(x_2)}{J_0(x_2)}}{x_1^2-x_2^2}.
\end{aligned} \tag{30}
$$

8. Conclusion

Beside giving procedure for the solution of the characteristic equation of a uniform magneto-ionic plasma column of circular cross section and computing the λ_g/λ_0 and P_p/P_a values for a few typical cases, our analysis has provided the following results, not given by the previous quasi-static analyses:

(1) Propagation may take place in the $\omega_p < \omega < \omega_b$ region, provided d/λ_0 is larger than a minimum cutoff value; in this case, at d/λ_0 values sufficiently larger than the cutoff value, power flow takes place mainly in the plasma $(P_p/P_a > 1)$.

2. In the $\omega > \omega_b, \omega_p$ region we may have not only backward waves, but also forward waves. Backward waves carry most of the power inside the plasma. Here too propagation is possible only over a finite range of d/λ_0 values.

3. When $\omega < \omega_p (\epsilon_3 < 0)$, in the ranges where computations have been performed, power flow in the first circularly symmetrical mode takes place mainly outside the plasma, whereas all other circularly symmetrical modes show large P_p/P_a ratios.

---

9. Appendix A

Regions I, II, and III of figure 1 have in common the following features:

(a) $0 < \epsilon_3 < 1$;

(b) δ_1^2 and δ_2^2 are always real;

(c) $\delta_2^2 \leq -1 (\delta_2^2$ versus α rises steadily from $-\infty$ at $\alpha = 1$ to -1 as $\alpha \to \infty)$;

(d) $-1 \leq \tau \leq 0$ (τ versus α rises steadily from -1 at $\alpha = 1$ to 0 as $\alpha \to \infty)$.

Inspection of figure 2 shows that in this case:

(a) When $\delta_1^2 > 0$ there are an infinite number of x_0 solutions of (8); the mth solution falls between $\nu^{(m)}(\delta_1)$ and $\mu^{(m)}(\delta_1)$. As $\delta_1^2 \to +\infty$ this solution vanishes $(x_0 \simeq X_0^{(m)}/\delta_1)$ and as $\delta_1^2 \to 0$ it becomes infinite $(x_0 \simeq X_1^{(m)}/\delta_1)$. In the $\tau = 0$ limit $(\alpha \to \infty)$ the x_0 solutions become equal to $\nu^{(m)}(\delta_1)$.

(b) When $\delta_1^2 < 0$, no solutions of (8) exist.

The above results determine the behavior of the x_0 versus α solutions, for given ϵ_1 and ϵ_3, if we know the characteristics of the δ_1^2 versus α curves. These are as follows:

(a) In region I, δ^2 drops from $+\infty$ at $\alpha = 1$ to 0 at α_0:

$$\alpha_0^2 = \epsilon_1 + \sqrt{(\epsilon_1 - 1)(\epsilon_1 - \epsilon_3)} = \epsilon_1 + \epsilon_2. \tag{A-1}$$

The parameter δ_1^2 becomes negative, when $\alpha > \alpha_0$.

(b) In region II, δ_1^2 is always negative.

(c) In region III, δ_1^2 is always positive and drops from $+\infty$ at $\alpha = 1$ to $\delta_\infty^2 = -\dfrac{\epsilon_3}{\epsilon_1} > 0$ as $\alpha \to \infty$.

10. Appendix B

Regions IV and V, when:

$$\alpha^2 \geq \alpha_i^2 = (\epsilon_1 - \epsilon_3)^{-1}(\epsilon_1 + \epsilon_3 - 2\epsilon_1\epsilon_3 + 2\sqrt{\epsilon_1\epsilon_3(\epsilon_1 - 1)(\epsilon_3 - 1)}) \tag{B-1}$$

have in common the following features:

(a) $\epsilon_3 < 0$;

(b) δ_1^2 and δ_2^2 are always real;

(c) δ_1^2 and δ_2^2 versus α are respectively the upper and lower branches of a curve, the shape of which is that of a deformed parabola with the vertex at α_i and two horizontal asymptots for $\alpha \to \infty$ $(\delta_1^2 \to \delta_\infty^2 = -\epsilon_3/\epsilon_1$ and $\delta_2^2 \to -1)$.

(d) $0 \leq \tau \leq 1$ (τ versus α drops from 1 at α_i to 0 as $\alpha \to \infty$).

Inspection of figure 3 shows that in this case:

(a) When $\delta_1^2 > 0$, there is an infinite number of solutions. The smallest x_0 (first solution) falls between zero and $\nu^{(1)}(\delta_1)$; as $\delta_1 \to 0$, it remains then finite. All the other x_0 solutions rise instead to infinity as $\delta_1^2 \to 0$, because the mth solution always falls between $X_1^{(m-1)}/\delta_1$ and $X_0^{(m)}/\delta_1$, if $\delta_2^2 < 0$. In the $\tau = 0$ limit ($\alpha \to \infty$) the x_0 solutions become equal to $\nu^{(m)}(\delta_\infty)$. In the $\tau = 1$ limit ($\alpha = \alpha_i$, $\delta_1^2 = \delta_2^2$), all the solutions go to infinity, except the first one which remains finite; in this limit (8) becomes an identity and the solution is given by the equation:

$$[\partial(gF)/\partial\delta]_{\alpha=\alpha_i} = 0. \tag{B-2}$$

(b) When $-\epsilon_3^2 \le \delta_1^2 < 0$, there is always one solution alone. This solution falls between zero and $\nu^{(1)}(\delta_1)$, and becomes equal to $\nu^{(1)}(\delta_\infty)$, as $\tau \to 0$.

(c) When $\delta_1^2 < -\epsilon_3^2$, there is one solution or no solutions depending on τ being larger or smaller than:

$$\tau_0 = \frac{1+|\delta_2|}{1+|\delta_1|} \frac{\epsilon_3 + |\delta_1|}{\epsilon_3 + |\delta_2|} \tag{B-3}$$

As $\tau \to \tau_0$, $x_0 \to \infty$.

Here too the x_0 versus α behavior can be derived from the above results, whenever the characteristics of the δ_1^2 versus α curves are known. The basic features of these curves are

(a) In region IV, $\delta_\infty^2 > 0$, so that there is always one region extending up to $\alpha = \infty$, where $\delta_1^2 > 0$. This region is the entire $\alpha \ge \alpha_i$ range, when:

$$\epsilon_3 \le \epsilon_3^0 = \frac{1}{2}\left(1 - 3\epsilon_1 - \sqrt{9\epsilon_1^2 - 10\epsilon_1 + 1}\right) \tag{B-4}$$

and is the $\alpha \ge \alpha_0$ range [see (A-1)], when $\epsilon_3 > \epsilon_3^0$.

(b) In region V, $\delta_\infty^2 < 0$ and then $\delta_1^2 < 0$ always. When $\delta_\infty^2 < -\epsilon_3^2$, no solutions exist as $\alpha \to \infty$, because $\tau = 0 < \tau_0$; in this case, continuity and regularity suggest, as confirmed by extensive numerical computations, that no solutions exist at any α value. Propagation is then possible only if $\epsilon_1\epsilon_3 > 1$ namely in the region:

$$\begin{cases} -\infty < \epsilon_1 < -1 \\ \epsilon_1 < \epsilon_3 < 1/\epsilon_1. \end{cases} \tag{B-5}$$

11. Appendix C

Regions IV and V, when $\alpha^2 < \alpha_i^2$, have in common the following features:

(a) $\epsilon_3 < 0$;

(b) δ_1^2 and δ_2^2 are complex conjugates;

(c) τ is a complex number, and $|\tau| = 1$.

It is convenient to transform (8) into an equation of only real quantities. For this purpose, recalling that Bessel functions of complex conjugate arguments are complex conjugates, we write:

$$\left.\begin{aligned}
\delta_{1,2}^2 &= |\delta|^2 \exp(\pm 2j\Theta) \\
g_{1,2} &= |g| \exp(\pm j\vartheta) \\
J_0(\delta_{1,2}x_0) &= S_0(|\delta|x_0, \Theta) \exp[\pm j\psi_0(|\delta|x_0, \Theta)] \\
J_1(\delta_{1,2}x_0) &= S_1(|\delta|x_0, \Theta) \exp[\pm j\psi_1(|\delta|x_0, \Theta)].
\end{aligned}\right\} \tag{C-1}$$

Equation (8) becomes:

$$\frac{\epsilon_3}{|\delta|^2}\frac{S_1^2}{S_0^2}+\frac{K_1^2(x_0)}{K_0^2(x_0)}=-\frac{1}{|\delta|}\frac{S_1}{S_0}\frac{K_1(x_0)}{K_0(x_0)}\left[\epsilon_3\frac{\sin\left[(\vartheta+\Theta)-(\psi_1-\psi_0)\right]}{\sin\vartheta}+\frac{\sin\left[(\vartheta-\Theta)+(\psi_1-\psi_0)\right]}{\sin\vartheta}\right]. \quad \text{(C-2)}$$

When an x_0 solution exists in the $\alpha > \alpha_i$ region and it ends at α_i with a finite value, then this solution has a smooth continuation in the $\alpha < \alpha_i$ region. The x_0 solution increases in this case as α decreases and becomes infinite at the α root of the equation:

$$\frac{|\delta|^2+\epsilon_3}{|\delta|}=\epsilon_3\frac{\cos(\vartheta+\Theta)-\cos(\vartheta-\Theta)}{\sin\vartheta}. \quad \text{(C-3)}$$

12. References

Akhiezer, A. I., et al., High-frequency plasma oscillations, Proc. II U.N. Int. Conf. Peaceful Uses of Atomic Energy **31**, 99–111 (United Nations, Geneva, 1958).

Allis, W. P., Motions of ions and electrons, Handbuch der Physik **XXI**, 383–444 (Springer-Verlag, Berlin, 1956).

Epstein, P. S., Theory of wave propagation in a gyromagnetic medium, Rev. Mod. Phys. **28**, 3–17 (Jan. 1956).

McLachlan, N. W., Bessel Functions for Engineers (Clarendon Press, Oxford, 1955).

Schumann, W. O., Über die Ausbreitung elektrischer Wellen längs einer dielektrisch begrenzten Plasmaschicht mit einem longitudinalem Magnetfeld, Z. Angew. Phys. **10**, 26–31 (1958).

Smullin, L. D., and P. Chorney, Propagation in ion loaded waveguides, Proc. Symp. Electronic Waveguides, pp. 229–247 (Polytechnic Press, Brooklyn, 1958).

Trivelpiece, A. W., and R. W. Gould, Space charge waves in cylindrical plasma columns, J. Appl. Phys. **30**, 1784–1793 (Nov. 1959).